Reaction Chemistry & Engineering

ROYAL SOCIETY OF CHEMISTRY

PAPER

View Article Online
View Journal

Cite this: DOI: 10.1039/d5re00333d

Model based process optimization for nanoparticle precipitation

Andrea Gilch, †[a] Adeel Muneer,†[bc] Jana Dienstbier[a] and Lukas Pflug [bc]

This study introduces a derivative-based optimization framework for the controlled synthesis of nanoparticles, with a focus on achieving target particle size distributions *via* dynamic manipulation of reactant inflow during precipitation. The key novel aspects of our approach include coupling population balance equations (PBE)-which accounts for nucleation and growth phenomena-with a prior first-order reduction reaction formulated using the exact Method of Moments (eMoM), and implementing a discretize-then-optimize approach for efficient computation of parameter sensitivities, enabling effective optimization of the time-dependent inflow profile. The objective is to minimize the variance in particle size while ensuring a prescribed mean diameter. Numerical case studies explore the role of process constraints and regularization strategies in control performance. The following quantitative results highlight the effectiveness of our approach: first, the optimized time-varying inflow profiles significantly outperform constant-rate strategies. Within the size range $\mu_D \pm 0.1\mu_D$, the optimal control yields nanoparticles with a purity exceeding 99%, compared with about 77% for the most effective constant control. Furthermore, the framework remains robust under variations in process parameters, sustaining performance despite limits on maximum inflow rate and total synthesis time. This framework offers a systematic and computationally tractable approach to optimizing transient operating conditions in nanoparticle synthesis, with strong potential for industrial application.

Received 31st July 2025,
Accepted 10th December 2025

DOI: 10.1039/d5re00333d

rsc.li/reaction-engineering

1 Introduction and problem definition

Nanoparticle research has received significant attention since the last century because nanoparticles have many innovative applications, such as in biomedicine,[1] optics,[2] or agriculture,[3] where small changes in the shape and structure of particles have a strong influence on their properties. Quantum dots displays and solar technologies are two prominent examples[4,5] as their optical properties are strongly influenced by the size of embedded nanoparticles.[6–10] The ability to produce nanoparticles with a desired size and narrow particle size distribution is thus of great interest.

Consequently, optimizing process conditions to tailor particle size distributions is essential to obtain high-quality products. For predefined particle systems, chemical engineers often experimentally investigate process conditions using their domain knowledge.[11] Furthermore, statistical methods such as the design of experiment (DoE) can be incorporated to systematically investigate the influence of multiple factors on the outcome of a process.[12–14] However, these procedures require a predefined experimental layout to explore the effects of multiple factors, which can become impractical when the number of parameters increases. This can lead to extensive experimental runs, especially in systems with many interacting variables, such as, *e.g.*, in a synthesis process. In addition, DoE is often static, relying on assumptions about parameter interactions. Once experiments are designed and conducted, adjustments require additional runs of experimentation. Thus, a structured exploration of the space of possible process conditions on a model basis, combined with the knowledge of chemical engineers, might be suitable for a small number of process parameters. Following this idea, derivative-free optimization techniques can be a powerful tool to optimize processes based on a small number of control parameters.[15] Furthermore, multiple publications follow the idea of process optimization as a closed-loop system directly on the basis of experiments and measurements, in recent works mostly relying on techniques from machine learning.[16–20] For these attempts, optimizing time-dependent controls in its full generality is not admissible due to the high-dimensional optimization space accompanied by time-consuming function evaluation, *i.e.*, running experiments and characterization procedures.

[a] *Friedrich-Alexander-Universitat Erlangen-Nurnberg (FAU), Department of Data Science (DDS), Professorship of Optimization under Uncertainty & Data Analysis, Nurnberger Strase 74, 91052 Erlangen, Germany.*
E-mail: jana.dienstbier,andrea.gilch@fau.de
[b] *Friedrich-Alexander Universitat Erlangen-Nurnberg (FAU), Department of Mathematics, Chair of Applied Mathematics (Continuous Optimization), Cauerstrase 11, 91058 Erlangen, Germany*
[c] *Friedrich-Alexander Universitat Erlangen-Nurnberg (FAU), Competence Center Scientific Computing (FAU CSC), Martensstrasse 5a, 91058 Erlangen, Germany.*
E-mail: adeel.muneer,lukas.pflug@fau.de
† These authors contributed equally to this manuscript.

To achieve higher precision in process control, time-dependent control strategies become relevant. So far, these have been out of reach for synthesis processes, as previously mentioned approaches cannot be applied effectively. To close this gap, this study develops a derivative-based framework for optimizing controlled nanoparticle synthesis. Our objective is to achieve target particle size distributions by dynamically controlling reactant inflow during precipitation, minimizing size variance while ensuring a prescribed mean diameter.

The key contributions of our approach include coupling Population Balance Equations (PBE) with a prior first-order reduction reaction to extend the model's applicability, formulating the problem using the exact Method of Moments (eMoM) to achieve high precision and computational efficiency and implementing a discretize-then-optimize approach to efficiently compute parameter sensitivities. A key technical challenge has been the numerical formulation itself. Traditional finite-volume methods (FVM) are inherently non-differentiable with respect to control variables when flux limiting schemes are employed to suppress numerical diffusion. This non-differentiability prevents the direct computation of gradients, making gradient-based optimization infeasible. The new approach overcomes this limitation by enabling accurate gradient evaluation, allowing control strategies to be optimized in ways that were previously impractical.

A significant advantage, in addition to its novelty in time-dependent control, is the scheme's broad applicability for optimizing diverse process conditions, such as temperature[21–24] and pH value,[25,26] offering strong potential for industrial application by improving product quality and process efficiency.

In a nutshell, we present a derivative-based optimization framework based on the idea of eMoM as introduced in Pflug *et al.*[27] The scheme follows the concept of first discretize, then optimize, see, for instance, Hinze and Rösch.[28] We thus state an efficient discretization scheme based on eMoM adapted from Pflug *et al.*[27] as well as Bänsch *et al.*[29] and then compute the sensitivities of the discretized version. We study the process optimization strategy using an academic example closely related to the model derived in Wang *et al.*[30] for indium phosphide quantum dot (InP QD) synthesis.

As examples, we are aiming to find the rate u of adding new precursor to the system during the synthesis process, which minimizes at the final time $T > 0$, *i.e.*, after the precipitation approximately stops, the variance of the resulting particle size distribution while matching the desired mean diameter μ_D:

$$\min_{u \in \mathcal{U}_{ad}} \mathrm{Var}[q(T,\cdot)] \quad \text{s.t. } E[q(T,\cdot)] = \mu_D, \tag{1}$$

where q solves the PBE describing nucleation ($\mathcal{N}$) and size-dependent growth ($\mathcal{G}$) of nanoparticles (NPs), including a first-order reduction reaction model.

The first-order reaction is determined by the following equations:

$$\dot{c}_0(t) = u(t) - k_r c_0(t) \quad \forall t \in [0,T] \tag{2}$$

$$c_0(0) = 0 \tag{3}$$

$$\dot{\bar{c}}(t) = k_r c_0(t) \qquad \forall t \in [0,T] \tag{4}$$

$$\bar{c}(0) = 0 \tag{5}$$

Furthermore, the PBE read as follows:

$$q(t,x)_t = -(\mathcal{G}(c(t),x)q(t,x))_x \quad \forall t \in [0,T], x > x_n \tag{6}$$

$$q(t,x_n) = \frac{\mathcal{N}(c(t))}{\mathcal{G}(c(t),x_n)} \qquad \forall t \in [0,T] \tag{7}$$

$$q(0,x) = 0 \qquad \forall x > x_n, \tag{8}$$

with inflow rate of precursor $u \geqq 0$, reduction constant $k_r > 0$ and nucleation size $x_n > 0$. Together with the equation for conservation of mass, which couples the concentration of the relevant species c, the total concentration $\bar{c}$ of this species in the precipitator, and the volume of the precipitated NPs, we obtain the following relation:

$$c(t) = \bar{c}(t) - \frac{\pi\rho}{6M_P}\int_{x_n}^{\infty} x^3 q(t,x)\mathrm{d}x \quad \forall t \in [0,T], \tag{9}$$

with M_P describing the molar mass and ρ the particle density.[29] It is worth mentioning that eqn (9) underlies nonlocal balance laws, which means that the observed kinetics depend nonlocally on the solution q. An overview of recent advances of nonlocal balance laws is provided by Keimer and Pflug,[31] Coclite *et al.*[32,33] Obviously, a truly narrow particle size distribution (PSD) with mean at μ_D and standard deviation approximately 0 minimizes this functional. We aim to tackle this optimization problem with a time-dependent control variable by reformulating the PBE in terms of eMoM. The idea is capable of handling any objective functional consisting of a nonlinear but differentiable combination of scalar products of the solution q, the control u, and functions in L^p for $p \in (1, \infty)$. For the sake of simplicity, we restrict ourselves to the objective functional stated in eqn (1).

The uniqueness of solutions to the PBE was shown in Pflug[34] and Keimer *et al.*,[35] the differentiability of the PBE and the objective functional with respect to the control was shown in Spinola.[36]

Structure of the paper

Section 2 presents the model's foundation, its validation based on InP QD synthesis, its applicability to other industrial processes, and its inherent limitations. In section 3 we

reformulate the optimization problems in terms of the exact Method of Moments and discretize the resulting fixed-point problem (FPP). In section 4, we introduce a range of possible constraints and regularizations, followed by the sensitivity analysis, *i.e.*, the computation of derivatives of the discretized FPP and objective functionals in section 5. Numerical examples illustrating the performance of the proposed scheme are provided in section 6, and a conclusion in section 7.

2 Applicability of the model

For this study, our approach is based on the model investigated by Wang *et al.*,[30] who adopted the underlying nucleation and growth kinetics from established models by Mersmann *et al.*[37] which are also used *e.g.*, in Schikarski *et al.*[38] Wang *et al.*[30] rigorously validated the model against experimental data for InP QD synthesis and demonstrated that it accurately predicts particle size distributions over process time. We adapt this well-established model to an academic case that closely parallels the InP QD synthesis process, incorporating similar nucleation and growth kinetics within a generalized optimization framework. To maintain experimental verification, the admissible ranges for the process controls are taken from.[30]

Moreover, the model's ability to accommodate a variety of process conditions (see section 6) further highlights its robustness. Despite its robustness, our model is subject to certain inherent limitations:

Nucleation and growth kinetics: although the framework is based on a validated model for InP QDs, it employs widely applicable nucleation and growth kinetics.[37] More generally, there are only two key requirements for these kinetics: they must be differentiable with respect to concentration and, if relevant, the control variable; and the growth kinetics must be expressible as the product of a function depending solely on concentration (and possibly the control variable) and a monomial in the particle size. The latter condition is trivially satisfied for the classically used diffusion- or reaction-limited kinetics.

Precursor chemistry: in this work, we assumed that the precursor chemistry can be represented by a first-order reduction reaction (2)–(5). However, this formulation is flexible, thus $\bar{c}(t)$ from eqn (9) can be replaced by any precursor chemistry that is analytically solvable and the corresponding derivative is available.

Although our study is based on a model validated for InP QD synthesis, the proposed optimization framework is broadly applicable to other industrial processes, including the anti-solvent precipitation of active pharmaceutical ingredients (APIs). For poorly soluble drugs such as ibuprofen, precise control of particle size and distribution is essential for tuning dissolution rates and bioavailability. Our derivative-based framework offers a systematic alternative to experimental trial-and-error by enabling the design of time-dependent inflow profiles for ibuprofen solutions into anti-solvents. By adapting nucleation and growth kinetics to the specific chemistry of ibuprofen crystallization,[39–41] the framework can identify optimal feeding strategies that produce nanoparticles with the desired mean size and minimal variance, thereby enhancing both product quality and process efficiency.

3 Exact method of moments

The basic idea of eMoM is – as prescribed in ref. 27 – to reformulate the PBE in terms of the concentration only. The important advantages of this method are on the one hand: high precision due to non-smoothing and less run time as compared to the well-known finite volume scheme (FVS). In addition, eMoM gives access to the full particle size distribution and not only to its moments. However, most importantly for this contribution, the numerical approximations of eMoM are, by construction, differentiable.

By solving the reduction reaction differential (2)–(5) analytically, we obtain the following

$$\bar{c}(t) = \int_0^t \left(1 - e^{-k_r(t-\tau)}\right) u(\tau) \mathrm{d}\tau. \tag{10}$$

As derived in ref. 35 and used in ref. 27, instead of solving the PBE (6)–(8) together with the mass balance eqn (9), we can solve the following fixed point problem:

$$c(t) = \gamma_1 \bar{c}(t) - \frac{\pi\rho}{6M_P} \int_0^t (\xi_c[\tau, x_n](t)) \mathcal{N}(c(\tau)) \mathrm{d}\tau, \tag{11}$$

along with the characteristics ξ_x solving:

$$\partial_3 \xi_c[t,x](\tau) = \mathcal{G}(c(\tau), \xi_c[t,x](\tau)) \tag{12}$$

$$\xi_c[t, x](t) = x, \tag{13}$$

for all t, $\tau \in [0, T]$ and $x > x_n$ where the index c for ξ emphasizes the concentration dependence of the characteristics. The FPP presented in eqn (11) is always an exact reformulation of the PBE and the mass balance equation. However, from a computational point of view, it is beneficial to the original PBE if the equation for the characteristics, *i.e.*, eqn (12) and (13) can be solved analytically.

In the case of $\mathcal{G}$ being a product of a solely concentration-dependent non-negative function and a monomial of the size, *i.e.*, there exist $n \in \mathbb{N}$ and $\mathcal{G}_0$ s.t.

$$\mathcal{G}(c, x) = x^n \mathcal{G}_0(c) \quad \forall x \geq x_n, \tag{14}$$

the following analytical solution of eqn (12) and (13) is obtained for $n \neq 1$ by:

$$\xi_c[t,x](\tau) = \left(x^{1-n} + (1-n)\int_t^\tau \mathcal{G}_0(c(s))\mathrm{d}s\right)^{\frac{1}{1-n}}. \tag{15}$$

While for $n = 1$, we get the following:

$$\xi_c[t,x](\tau) = x\exp\left(\int_t^\tau \mathcal{G}_0(c(s))\mathrm{d}s\right). \tag{16}$$

This is in line with eqn (15) when passing $n \to 1$ by the definition of the exponential function.[42] We omit the special case $n = 1$ since—to the author's knowledge—this is of no practical relevance in nanoparticle synthesis. Substituting eqn (15) into eqn (11) for the case $n \neq 1$, we obtain the following FPP solely in terms of the concentration c

$$c(t) = \bar{c}(t) - \frac{\pi\rho}{6M_P}\int_0^t \mathcal{N}(c(\tau))\left(x_n^{1-n} + (1-n)\int_\tau^t \mathcal{G}_0(c(s))\mathrm{d}s\right)^{\frac{3}{1-n}}\mathrm{d}\tau. \tag{17}$$

3.1 Moment analysis

In order to evaluate the stated objective functional given by eqn (1) and, in general, all objective functionals formulated with moments of the PSD at the final time, we derive a formula for the mth moment of the number density distribution $q(T,\cdot)$ as a function of the concentration. Considering the solution formula[27] Thm. 2.2. with $\alpha = 0$, and $q_0 = 0$, we obtain

$$q(t,x) = \begin{cases} \dfrac{\mathcal{N}(c(\tau))\partial_2\xi_c[t,x](\tau)}{x_n^n\mathcal{G}_0(c(\tau))} & \text{for } x_n \le x \le \xi_c[0,x_n](t), \\ 0 & \text{else,} \end{cases} \tag{18}$$

where $\tau = \tau_{t,x}$ satisfies $\xi_c[t,x](\tau_{t,x}) = x_n$.

The mth moment y_m of the solution at the final time T satisfies:

$$y_m = \int_{x_n}^\infty q(T,x)x^m\mathrm{d}x \tag{19}$$

$$= \int_{x_n}^{\xi_c[0,x_n](T)} \frac{\mathcal{N}(c(\tau))\partial_2\xi_c[T,x](\tau)}{x_n^n\mathcal{G}_0(c(\tau))}x^m\mathrm{d}x. \tag{20}$$

Moreover, by substitution of $x = \xi_c[\tau,x_n](T)$ as a function of τ, by integration of it's derivative $\partial_1\xi_c[\tau,x_n](T)$, and by using the following property of the characteristics, see ref. 35 Lem. 2.7. Eq 2.11. $\partial_2\xi_c[T,\xi_c[\tau,x_n](T)](\tau) = (\partial_2\xi_c[\tau,x_n](T))^{-1}$, we obtain:

$$= \int_T^0 \frac{\mathcal{N}(c(\tau))}{x_n^n\mathcal{G}_0(c(\tau))}(\xi_c[\tau,x_n](T))^m\frac{\partial_1\xi_c[\tau,x_n](T)}{\partial_2\xi_c[\tau,x_n](T)}\mathrm{d}\tau. \tag{21}$$

Eventually, by using the identity, see ref. 34 Lem. 2.6. Item 1.: $\partial_1\xi_c[T,x_n](\tau) + x_n^n\mathcal{G}_0(c(\tau))\partial_2\xi_c[T,x_n](\tau) = 0$, we get the final result for y_m:

$$= \int_0^T \mathcal{N}(c(\tau))(\xi_c[\tau,x_n](T))^m\mathrm{d}\tau. \tag{22}$$

3.2 Discretization

Subsequently, we approximate the reduction reaction solution eqn (10), the FPP eqn (17), and the mth moment eqn (22) to derive a suitable numerical scheme. For this, we assume a discretization of the time-horizon $[0, T]$ by $t_k \in [0, T]$ $\forall k \in \{1, \ldots, N_t\}$ with $N_t \in \mathbb{N}$ being the number of time discretization points and

$$0 = t_1 < t_2 < \ldots < t_{N_t} = T.$$

For the sake of simplicity, we define

$$\delta_k := t_{k+1} - t_k \quad \forall k \in \{1, \ldots, N_t - 1\}.$$

For the reduction reaction, we derive the following approximation:

$$\bar{C}_k = \sum_{\ell=1}^{k-1} U_\ell\left(\delta_\ell + \frac{1 - e^{k_r\delta_\ell}}{k_r e^{k_r(t_k - t_\ell)}}\right), \tag{23}$$

with $\bar{C}_k \approx \bar{c}(t_k)$, and $U_\ell \approx u(t_\ell)$. Especially, in the case of a piecewise constant control u on each interval $[t_k,t_{k+1})$ $\forall k$, eqn (23) is exact. Next, we obtain the following discretization for the FPP (compare ref. 27 and 29):

$$C_{k+1} = C_k + (\bar{C}_{k+1} - \bar{C}_k) - \frac{\pi\rho}{6M_P}\mathcal{N}(C_k)\delta_k\mathsf{G}_{k,k}{}^3 - \frac{\pi\rho}{6M_P}\sum_{\ell=1}^{k-1}\mathcal{N}(C_\ell)\delta_\ell\left(\mathsf{G}_{\ell,k}{}^3 - \mathsf{G}_{\ell,k-1}{}^3\right), \tag{24}$$

$$C_1 = \bar{C}_1, \tag{25}$$

with $C_k \approx c(t_k)$ $\forall k \in \{1, \ldots, N_t\}$. Furthermore, the approximated characteristics are defined as:

$$\mathsf{G}_{\ell,k} := \left(x_n^{1-n} + (1-n)\sum_{m=\ell}^{k}\mathcal{G}_0(C_m)\delta_m\right)^{\frac{1}{1-n}}. \tag{26}$$

Combining all N_t eqn (24) and (25) (for $k = 1, \ldots, N_t$), the latter can be written in a compact form as:

$$F(\bar{C},C) = 0, \tag{27}$$

with the mapping F: $\mathbb{R}^{N_t} \times \mathbb{R}^{N_t} \mapsto \mathbb{R}^{N_t}$. The full function F and its derivative is defined in the SI, see section S1 and S2.

Lastly, the mth moment y_m can be approximated as follows:

$$Y_m = \sum_{\ell=1}^{N_t-1}\mathcal{N}(C_\ell)\delta_\ell\,\mathsf{G}_{\ell,N_t-1}^m. \tag{28}$$

4 Regularization and admissible controls

In order to be able to implement the optimized conditions in a process setup, a set of constraints might be needed. For this, we introduce a range of constraints and regularization possibilities, which are then also numerically studied in section 6.

4.1 Admissible controls

The set of admissible controls $\mathcal{U}_{\text{ad}}$ (see eqn (1)) can incorporate various constraints, *e.g.*, due to technical reasons of the precipitation process setup. Canonically, these are given by a desired total educt mass, limits on the inflow rate, as well as limited changes of the inflow rate. All these have in common that they can be formalized as linear constraints in terms of the process control variable.

Desired total educt mass. A desired total mass m_{tot} can be prescribed by the integral over the control u, which results in the discretized manner as the following linear equality constraint:

$$\sum_{i=1}^{N_t-1} U_i \delta_i = m_{\text{tot}}, \tag{29}$$

or if only a lower bound on the product mass has to be ensured, this can be postulated as an inequality constraint.

Limits on the inflow rate. To implement limitations on the flow rate, *i.e.*, bounds on u, the discretized version of u has to be bounded from above, *i.e.*, we obtain $N_t - 1$ linear inequality constraints:

$$U_k \leq u_{\max} \quad \forall k \in \{1, \ldots, N_t - 1\}, \tag{30}$$

with $u_{\max} > 0$ as the upper bound on the flow rate.

Limited changes of the inflow rate. For prescribing restrictions on the change of the inflow rate u, $|\dot{u}|$ has to be bounded. In discretized form, this results in $2(N_t - 2)$ linear inequality constraints, *i.e.*

$$|U_k - U_{k+1}| \leq \delta_k B_{\dot{u}} \quad \forall k \in \{1, \ldots, N_t - 2\}, \tag{31}$$

with $B_{\dot{u}} > 0$ as an upper bound on the change of the inflow rate.

4.2 Regularization

To ensure a desired smoothness of the optimal control u, penalizing its L^2-norm or the L^2-norm of its derivative—*i.e.*, the H^1-semi-norm—is the canonical way. For this, we describe and later study the impact of these two penalizations on the optimized process control. In a discretized form, one has to add for α_0, $\alpha_1 \in \mathbb{R}_{>0}$ the following to the objective functional:

$$\alpha_0 \sum_{i=1}^{N_t-1} \delta_i {U_i}^2 + \alpha_1 \sum_{i=1}^{N_t-2} \delta_i^{-1} (U_i - U_{i+1})^2. \tag{32}$$

5 Sensitivity analysis

For an efficient optimization of the time-dependent inflow rate of new precursor in the nucleation and growth process, we calculate the derivative of the objective functional and the nonlinear constraint eqn (1) with respect to the control U. For this, we consider a generic functional J:

$$\partial_{U_k} J(C(\bar{C}(U))) = \partial_C J(C) \partial_{\bar{C}} C(\bar{C}) \partial_{U_k} \bar{C}(U), \tag{33}$$

with a slight abuse of notation, *i.e.* $C := C(\bar{C}(U))$, $\bar{C} := \bar{C}(U)$.

For instance, for an objective functional defined as a nonlinear function of a range of moments of the final PSD, *i.e.*

$$J(C) = \hat{J}(Y_1(C), \ldots, Y_m(C)), \tag{34}$$

its derivative is calculated by the chain rule, *i.e.*

$$\nabla J(C) = \sum_{i=1}^{m} \partial_i \hat{J}(Y_1(C), \ldots, Y_m(C)) \nabla Y_i(C). \tag{35}$$

As example, the objective functional (*i.e.*, the variance of the PSD at final time) as well as the constraint (*i.e.*, a desired mean size at final time) as defined in eqn (1) and its derivatives are stated in the SI, see section S3 and S4. For the derivative of the moments (see eqn (28)), we obtain the following formula:

$$\partial_{C_i} Y_m = \begin{cases} \mathcal{N}_i' \delta_i \mathsf{G}_{i,k-1}^m + m \mathcal{G}_i' \delta_i \sum_{\ell=1}^{i} \mathcal{N}_\ell \delta_\ell \mathsf{G}_{\ell,k-1}^{m+n-1} & \text{if } i < k, \\ 0 & \text{else.} \end{cases} \tag{36}$$

The derivative of the concentration w.r.t. the total concentration $\bar{C}$ is a bit more involved as C is a function of $\bar{C}$ as it is the solution of the FPP, $F(\bar{C}, C(\bar{C})) = 0$ as defined in eqn (27). Thus $\partial_{\bar{C}} C(\bar{C})$ is given by the implicit function theorem (see, for instance ref. 43):

$$\partial_{\bar{C}} C(\bar{C}) = -(\partial_C F(\bar{C}, C))^{-1} \partial_M F(\bar{C}, C), \tag{37}$$

with $F(\bar{C}, C(\bar{C})) = 0$ (for the sake of simplicity, we omit the dependencies). For the derivative of the FPP mapping with respect to the first argument, we obtain the following.

$$\partial_{\bar{C}_i} F_k(\bar{C}, C) = \begin{cases} -1 & \text{for } i = k, \\ 1 & \text{for } i = k-1, \\ 0 & \text{else.} \end{cases} \tag{38}$$

While the formula for the derivative with respect to the second argument, *i.e.* $\partial_{C_i} F(\bar{C}, C)$, is due to readability stated in the SI (S3). Lastly, for the derivative of $\bar{C}$ w.r.t. U, *i.e.* the reduction reaction, we thus obtain:

$$\partial_{U_i} \bar{C}_k = \begin{cases} \delta_i + \dfrac{1 - e^{k_r \delta_i}}{k_r e^{k_r (t_k - t_i)}} & \text{for } i < k, \\ 0 & \text{else.} \end{cases} \tag{39}$$

The derivatives of the regularizations proposed in Section 4 are straightforward and thus not discussed here.

6 Numerical examples

For studying the proposed method, as well as the effect of process parameters, we consider the following growth and nucleation kinetics, which were inspired by ref. 37 and 38.

$$\mathcal{G}_0(c) := \begin{cases} k_g(c - c_{eq}) & \text{for } c > c_{eq}, \\ 0 & \text{else}, \end{cases}$$

$$\mathcal{N}(c) := \begin{cases} k_c^{(1)} \left(\frac{c}{c_{eq}}\right)^{\frac{7}{3}} \exp\left(-k_c^{(2)} \log\left(\frac{c}{c_{eq}}\right)^{-2}\right) & \text{for } c > c_{eq}, \\ 0 & \text{else}, \end{cases}$$

with the coefficients stated in Table 1.

To showcase the impact of a time-dependent process control, *i.e.*, the time-dependent inflow rate of precursor solution, we compare the obtained result to any constant control, *i.e.*, a constant inflow over a given time-horizon. In formulas, we compare the obtained final PSD for the optimized control to the final PSD obtained by constant controls parametrized by their total amount $\bar{m} \in \mathbb{R}_{>0}$ and time horizon $\bar{t} \in (0, T]$

$$u_{\bar{t},\bar{m}}(t) := \frac{\bar{m}}{\bar{t}} \chi_{(0,\bar{t})}(t). \tag{40}$$

In this study, two types of constant control were considered. The first constant control, corresponds to the maximum inflow rate u_{max} applied over the time required to add the full mass; here, no optimization is applicable, as both the inflow rate and total addition time are fixed. The second constant control, refers to a constant inflow rate chosen to achieve the target mean particle size μ_D. This rate was determined *via* a parameter sweep over possible inflow rates. Once selected, the resulting variance of the particle size distribution is fixed, since the inflow rate and total addition time are fully determined by the target mean size and total mass.

Both choices lead to significantly broader size distributions compared to the time-dependent optimal control and, in the case of a maximal inflow rate for short times, not even satisfying the desired mean size (compare Fig. 1, bottom figure, purple).

When comparing the quality of the resulting product, the difference becomes even more prominent. We compare in Fig. 2 the mass percentage of NPs in a defined size range around the desired size; in other words, we analyze the product purity for the resulting PSD for different purity thresholds. In formulas, we visualize:

$$Q(a) := \frac{\int_{\mu_D(1-a)}^{\mu_D(1+a)} x^3 q(T,x)\mathrm{d}x}{\int_{x_n}^{\infty} x^3 q(T,x)\mathrm{d}x}. \tag{41}$$

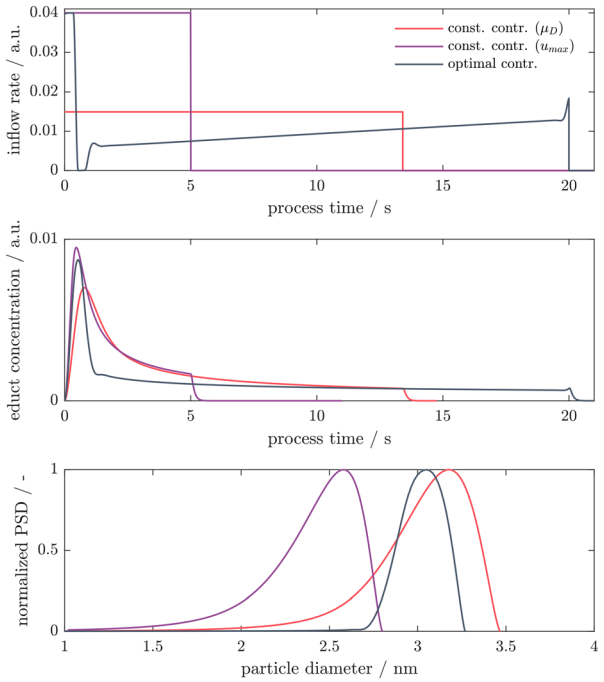

Fig. 1 Comparison of two constant controls (red and purple) with the optimized control (black). The constant controls are chosen in red: such that the final PSD possesses the desired mean size μ_D = 3 and in purple: to showcase a shorter injection time, showing that reducing the injection time reduces the mean size. This highlights the benefit of the time-dependent control, which clearly shows a smaller standard deviation of the final PSD.

For example, by computing the percentage of the mass of nanoparticles in the size range of $\mu_D \pm 0.1\mu_D$, the optimal control results in NPs with a purity of above 99% while the best constant control results in NPs with a purity of approximately 77%. This clearly shows the huge impact of time-dependent process controls on the resulting product quality.

In the following paragraphs, we discuss the effect of a range of constraints and parameters in the proposed optimization framework.

Final time

The effect of the final time of the control T_c is shown in Fig. 3 where T_c ranges from T_c = 10 to T_c = 30. By adjusting the final time, which is the moment when the inflow must cease, the 'structure' of the control is preserved. This structure consists of an initial short injection pulse to stimulate nucleation, followed by a brief pause before an almost linear increase in the injection

Table 1 Coefficients for the numerical example. The magnitude of the coefficients are inspired by the formation of indium-phosphate quantum dots[30]

Symbol	c_{eq}	k_g	$k_c^{(1)}$	$k_c^{(2)}$	$\frac{\pi\rho}{6M_P}$	k_r	μ_D	κ	T_c	u_{max}	M_P	ρ
Value	10^{-13}	10^{-7}	2×10^{-22}	10^4	2×10^1	5–20	3	10^{-2}–10^0	10–30	0.03–0.04	233.38	4500
Unit	mol l^{-1}	m l s^{-1} mol^{-1}	1 s^{-1}	—	mol m^{-3} l^{-1}	—	n m	—	s	m^3 s^{-1}	kg K mol^{-1}	kg m^{-3}

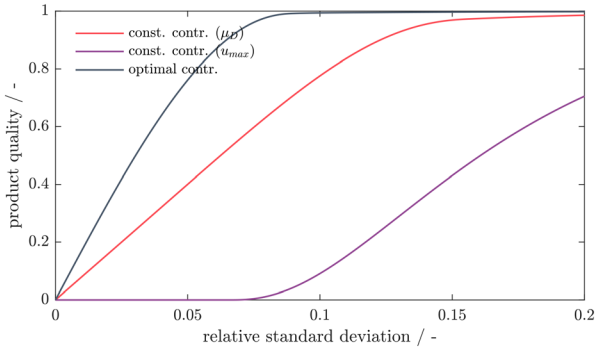

Fig. 2 Comparison of the product quality as defined in eqn (41) for different inflow rate profiles as described in Fig. 1. The best constant control possesses, *e.g.*, a 10% relative standard deviation, a product quality of only approximately 77%, whereas the product quality for the optimized control reaches above 99%.

rate that promotes growth. However, because of the limited time available to inject a predefined mass, the injection rate during the growth phase becomes too high, resulting in additional nucleation. This leads to a larger 'tail' of the PSD (particle size distribution) on the left. This effect is particularly pronounced for T_c = 10. Furthermore, increasing the final time from T_c = 20 (black) to T_c = 30 (purple) hardly reduces the standard deviation of the final PSD.

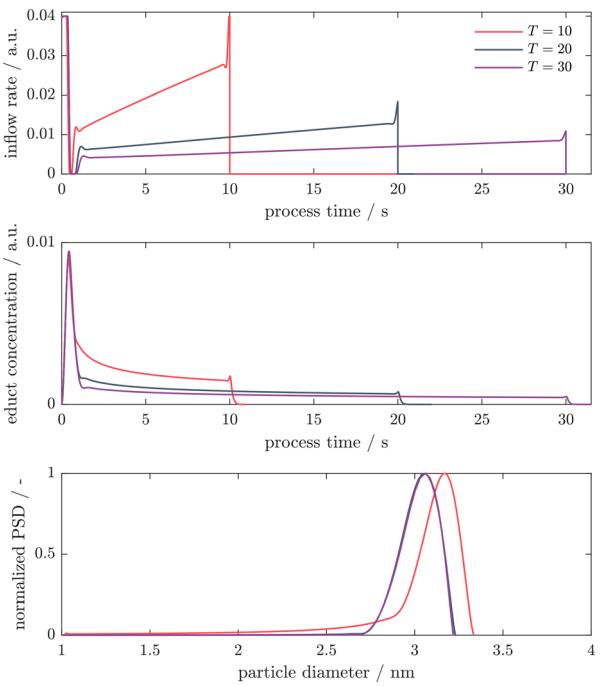

Fig. 3 Variation of final inflow time T_c from 10 to 30 while the upper bound u_{max} = 0.04 and regularization parameter $\kappa = 10^{-1}$ is chosen constant. There is a clear influence of shorter times, *i.e.* T_c = 10 on the width of the final PSD (red, lower figure) as the nucleation phase and growth phase cannot be "separated" as needed, whereas there is only a minor gain when increasing T_c from 20 to 30.

Bounds on u

The requirement for a restricted inflow rate could be linked to the experimental setup. In Fig. 4 the impact of a limited u_{max} ranging from 0.03 to 0.05 is illustrated. Within the selected range of bounds, the effect on the final PSD is minimal, exhibiting only a slight widening of the PSD as the upper bound decreases.

Reduction rate k_r

The reduction rate k_r (see eqn (2)) governs the rate at which the total concentration $\bar{c}$ (see eqn (4)) can rise and subsequently be depleted during particle formation. Increasing k_r enhances the controllability of the NP synthesis process by the addition of precursor solution and therefore results in a narrower PSD (Fig. 5).

H^1 penalization

Penalizing the H^1-norm of the control in the optimization setting regularizes the optimal control obtained. The effect can be seen in Fig. 6, where, with increasing penalization factor κ, the control becomes increasingly regularized.

7 Conclusion and outlook

The possibility of optimizing NP synthesis, including nanoparticle nucleation and size-dependent growth based on eMoM, was demonstrated. In addition to the PBE, a first-

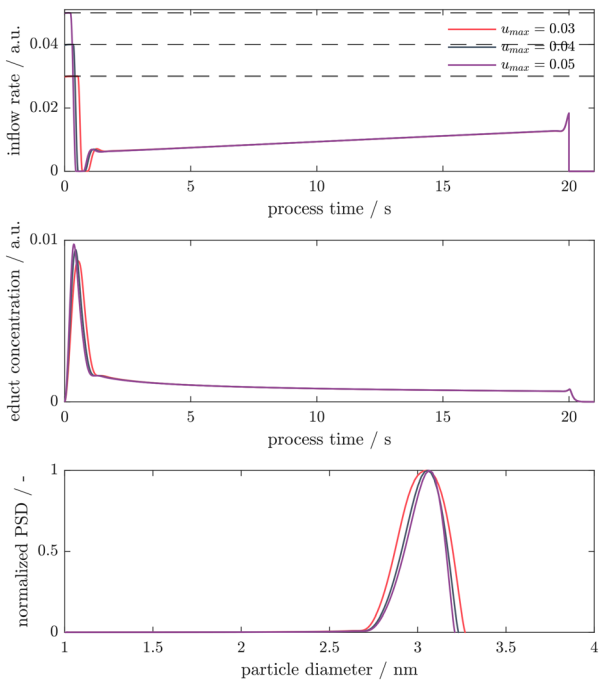

Fig. 4 Limiting the maximal inflow rate $u(t) \leq u_{max}\ \forall t \in [0, T]$. The effect on the final PSD (lower figure) is only minor and there is for decreasing u_{max} only a slight widening of the PSD visible. The final inflow time T_c = 20 and regularization parameter $\kappa = 10^{-1}$ are chosen to be constant.

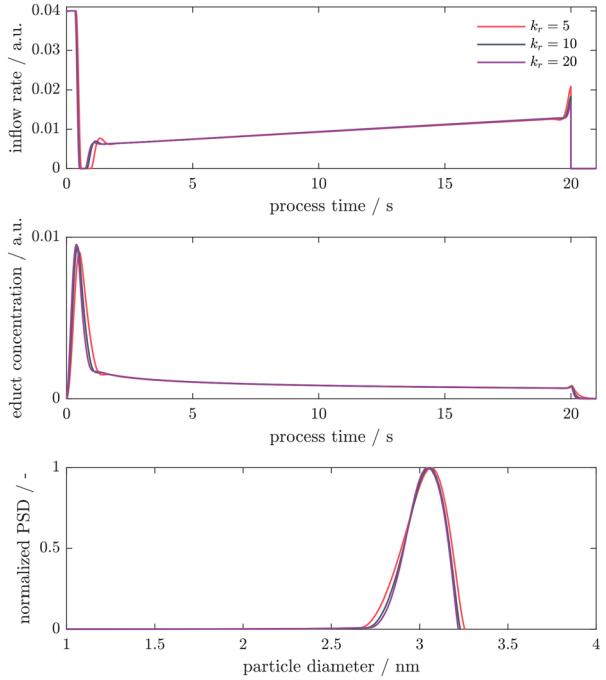

Fig. 5 The reduction rate was varied as $k_r \in \{5, 10, 20\}$. At lower reduction rates, the inflow rate is controlled more indirectly, leading to a sub-optimal reactant concentration profile and, as a result, a broader PSD.

order reduction reaction is included to enlarge the applicability of the stated results. The derived sensitivities to efficiently optimize time-dependent process controls strongly rely on the differentiability of the discretization of the fixed-point problem derived by eMoM. Based on an academic setting, inspired by commonly used nucleation and growth kinetics, the effects of the involved model parameters, regularizations, constraints, and discretization are studied in detail, demonstrating the suitability of the presented approach for optimizing nanoparticle precipitation processes.

Although this study focuses on optimizing the inflow rate for nanoparticle synthesis, the underlying framework is more general and can be adapted to optimize other time-dependent processes. In particular, the PBE and eMoM used in this study are broadly applicable to other nanoparticle systems. By tailoring the growth and nucleation kinetics to the specific chemistry, this framework can optimize the synthesis of a wide range of nanoparticle materials. In addition, process conditions such as temperature[21–24] and pH[25,26] play a critical role in nanoparticle synthesis, as they directly influence nucleation and growth kinetics. By extending the kinetic equations to incorporate both temperature and pH dependences, the framework can be adapted to optimize the time-dependent profiles of these variables. For pH-sensitive systems, this may require further additional equations to model pH dynamics within the reaction environment. Lastly, the flexibility of the framework enables the simultaneous optimization of multiple process variables. For example, both the inflow rate and the temperature profiles can be optimized at the same time, potentially providing even better control over the final particle size distribution. In future work, we aim to further investigate the generality of the proposed framework by applying it to different nanoparticle systems and extending it towards the optimization of multiple process variables.

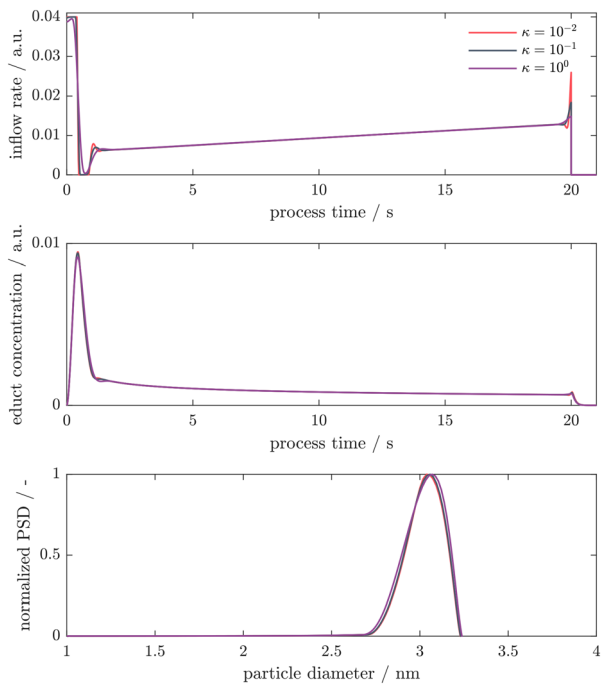

Fig. 6 Increasing the H^1-regularization from $\kappa = 10^{-2}$ to 10^0 results in a control with increasing regularity (left plot) and causes an increase in the standard deviation of the resulting PSD (lower figure). The final inflow time $T_c = 20$ and upper bound $u_{max} = 0.04$ are chosen to be constant.

Conflicts of interest

There are no conflicts to declare.

Data availability

Data for this article are available at ZENODO at https://doi.org/10.5281/zenodo.17950465.

Supplementary information (SI) is available. See DOI: https://doi.org/10.1039/d5re00333d.

Acknowledgements

The research was funded by the Deutsche Forschungsgemeinschaft (DFG, German Research Foundation) - Project-ID 416229255 - SFB 1411.

Notes and references

1 N. Millot, *Biomedical Applications of Nanoparticles*, MDPI, 2020.
2 A. Tiwari, *Solar Cell Nanotechnology*, Scrivener Publishing LLC, 2014.

3 N. Sozer and J. L. Kokini, *Trends Biotechnol.*, 2009, **27**, 82–89.
4 K. Bourzac, *et al.*, *Nature*, 2013, **493**, 283.
5 H. Zhao and F. Rosei, *Chem*, 2017, **3**, 229–258.
6 D. Segets, J. M. Lucas, R. N. Klupp Taylor, M. Scheele, H. Zheng, A. P. Alivisatos and W. Peukert, *ACS Nano*, 2012, **6**, 9021–9032.
7 M. Distaso, D. Segets, R. Wernet, R. K. Taylor and W. Peukert, *Nanoscale*, 2012, **4**, 864–873.
8 T. Akdas, J. Walter, D. Segets, M. Distaso, B. Winter, B. Birajdar, E. Spiecker and W. Peukert, *Nanoscale*, 2015, **7**, 18105–18118.
9 V. I. Klimov, *Nanocrystal quantum dots*, CRC Press, 2017.
10 A. M. Wagner, J. M. Knipe, G. Orive and N. A. Peppas, *Acta Biomater.*, 2019, **94**, 44–63.
11 P. Suchomel, L. Kvitek, R. Prucek, A. Panacek, A. Halder, S. Vajda and R. Zboril, *Sci. Rep.*, 2018, **8**, 4589.
12 S. Chowdhury, F. Yusof, M. O. Faruck and N. Sulaiman, *Procedia Eng.*, 2016, **148**, 992–999.
13 Z. Lalegani and S. Seyyed Ebrahimi, *Colloids Surf., A*, 2020, **595**, 124647.
14 E. M. Williamson, Z. Sun, L. Mora-Tamez and R. L. Brutchey, *Chem. Mater.*, 2022, **34**, 9823–9835.
15 D. Long, R. G. Finke and W. Bangerth, *ACS Appl. Nano Mater.*, 2024, **7**, 14090–14101.
16 B. L. Hall, C. J. Taylor, R. Labes, A. F. Massey, R. Menzel, R. A. Bourne and T. W. Chamberlain, *Chem. Commun.*, 2021, **57**, 4926–4929.
17 F. Mekki-Berrada, Z. Ren, T. Huang, W. K. Wong, F. Zheng, J. Xie, I. P. S. Tian, S. Jayavelu, Z. Mahfoud, D. Bash, K. Hippalgaonkar, S. Khan, T. Buonassisi, Q. Li and X. Wang, *npj Comput. Mater.*, 2021, **7**, 63–63.
18 K. Nathanael, S. Cheng, N. M. Kovalchuk, R. Arcucci and M. J. Simmons, *Chem. Eng. Res. Des.*, 2023, **193**, 65–74.
19 J. Park, Y. M. Kim, S. Hong, B. Han, K. T. Nam and Y. Jung, *Matter*, 2023, **6**, 677–690.
20 T. K. Takumi Ono, Y. Takebayashi and K. Sue, *J. Chem. Eng. Jpn.*, 2023, **56**, 2211125.
21 S. Sun and H. Zeng, *J. Am. Chem. Soc.*, 2002, **124**, 8204–8205.
22 D. A. Fleming and M. E. Williams, *Langmuir*, 2004, **20**, 3021–3023.
23 D. Mott, J. Galkowski, L. Wang, J. Luo and C.-J. Zhong, *Langmuir*, 2007, **23**, 5740–5745.
24 J. Zhang, R. W. Crisp, J. Gao, D. M. Kroupa, M. C. Beard and J. M. Luther, *J. Phys. Chem. Lett.*, 2015, **6**, 1830–1833.
25 Y. Qin, X. Ji, J. Jing, H. Liu, H. Wu and W. Yang, *Colloids Surf., A*, 2010, **372**, 172–176.
26 C.-C. Ho and S.-J. Ding, *J. Mater. Sci.: Mater. Med.*, 2013, **24**, 2381–2390.
27 L. Pflug, T. Schikarski, A. Keimer, W. Peukert and M. Stingl, *Comput. Chem. Eng.*, 2020, **136**, 106775.
28 M. Hinze and A. Rösch, *Constrained optimization and optimal control for partial differential equations*, Springer, 2012, pp. 391–430.
29 E. Bänsch, L. Pflug and T. Schikarski, *Chem. Eng. Res. Des.*, 2023, **190**, 814–828.
30 Z. Wang, N. E. Traoré, T. Schikarski, L. M. Stiegler, D. Drobek, B. A. Zubiri, E. Spiecker, J. Walter, W. Peukert and L. Pflug, *et al.*, *Chem. Eng. Sci.*, 2023, **281**, 119062.
31 A. Keimer and L. Pflug, *Numerical Control: Part B*, Elsevier, 2023, vol. 24, pp. 183–216.
32 G. M. Coclite, J.-M. Coron, N. De Nitti, A. Keimer and L. Pflug, *Ann. Inst. H. Poincaré C Anal. Non Linéaire*, 2022, **40**, 1205–1223.
33 G. M. Coclite, N. De Nitti, A. Keimer and L. Pflug, *Nonlinear Anal. Theory Method Appl.*, 2021, **211**, 112370.
34 A. Keimer and L. Pflug, *J. Differ. Equ.*, 2017, **263**, 4023–4069.
35 A. Keimer, L. Pflug and M. Spinola, *SIAM J. Math. Anal.*, 2018, **50**, 6271–6306.
36 M. Spinola, *PhD thesis*, Friedrich-Alexander-Universität Erlangen-Nürnberg (FAU), 2022.
37 A. Mersmann, K. Bartosch, B. Braun, A. Eble and C. Heyer, *Chem. Ing. Tech.*, 2000, **72**, 17–30.
38 T. Schikarski, M. Avila and W. Peukert, *Chem. Eng. J.*, 2021, **428**, 131984.
39 T. Schikarski, M. Avila, H. Trzenschiok, A. Güldenpfennig and W. Peukert, *Chem. Eng. J.*, 2022, **436**, 136195.
40 T. Schikarski, H. Trzenschiok, M. Avila and W. Peukert, *Chem. Eng. Technol.*, 2019, **42**, 1635–1642.
41 T. Schikarski, H. Trzenschiok, M. Avila and W. Peukert, *Powder Technol.*, 2022, **415**, 118032.
42 E. Maor, *e: The Story of a Number*, Princeton University Press, 2009, vol. 72.
43 S. G. Krantz and H. R. Parks, *The implicit function theorem: history, theory, and applications*, Springer Science & Business Media, 2002.